Journal of Power Sources 234 (2013) 217–222

Contents lists available at SciVerse ScienceDirect

Journal of Power Sources

journal homepage: www.elsevier.com/locate/jpowsour

$LiMn_{0.5}Fe_{0.5}PO_4$ solid solution materials synthesized by rheological phase reaction and their excellent electrochemical performances as cathode of lithium ion battery

Yan-Jun Zhong [a,b], Jun-Tao Li [b], Zhen-Guo Wu [a,b], Xiao-Dong Guo [a], Ben-He Zhong [a], Shi-Gang Sun [b,*]

[a] School of Chemical Engineering, Sichuan University, Chengdu 610065, China
[b] School of Energy Research, State Key Lab of Physical Chemistry of Solid Surfaces, College of Chemistry and Chemical Engineering, Energy Research School, Xiamen University, Xiamen 361005, China

HIGHLIGHTS

- Carbon coated $LiMn_{0.5}Fe_{0.5}PO_4$ solid solution is synthesized by rheological phase reaction.
- This process possesses simple technology, low energy consumption.
- Nanoplatelet particles are coated uniformly with carbon layer.
- The obtained $LiMn_{0.5}Fe_{0.5}PO_4$/C exhibit excellent rate capability and cycling performance.
- $LiMn_{0.2}Fe_{0.8}PO_4$/C and $LiMn_{0.8}Fe_{0.2}PO_4$/C are synthesized by the same route for the comparison.

ARTICLE INFO

Article history:
Received 21 July 2012
Received in revised form
31 October 2012
Accepted 13 January 2013
Available online 10 February 2013

Keywords:
Lithium manganese–iron phosphate
Nanoplatelet
Rheological phase reaction
Lithium ion battery
Electrochemical performances

ABSTRACT

Carbon coated $LiMn_{0.5}Fe_{0.5}PO_4$ solid solution materials ($LiMn_{0.5}Fe_{0.5}PO_4$/C) are synthesized by rheological phase reaction with stearic acid as carbon source, and characterized by X-ray diffraction (XRD), scanning electron microscopy (SEM), transmission electron microscopy (TEM), BET and TG/DTG. The results show that well-crystallized olivine structure $LiMn_{0.5}Fe_{0.5}PO_4$ nanoplatelets with no obvious impurity phase are obtained. The as-synthesized materials are served as cathode of lithium ion battery and investigated by galvanostatic charge/discharge tests. The results demonstrate that, in comparison with the LMFP materials of different Mn:Fe ratio ($LiMn_{0.2}Fe_{0.8}PO_4$/C and $LiMn_{0.8}Fe_{0.2}PO_4$/C) synthesized by the same route of rheological phase reaction, the $LiMn_{0.5}Fe_{0.5}PO_4$/C exhibit excellent rate specific capability, and can deliver discharge capacity of 138, 99, 80, 72, 67 and 55 mAh g^{-1} at respectively 0.1, 1, 5, 10, 15 and 20C rates. Moreover, the electrode possesses good cycle stability. A specific capacity of 100 mAh g^{-1} at 1C after 300 cycles of charge–discharge at room temperature is reached, which represents 95% of capacity retention. The significantly improved electrochemical performances of the $LiMn_{0.5}Fe_{0.5}PO_4$/C cathode are attributed to the uniformly distributed particles and the enhancement of conductivity that is originated from the surface coating of carbon on primary particles.

1. Introduction

Lithium-ion battery is currently the widest and most promising electrochemical energy storage technology for many important applications, such as portable electronic consumer devices, electric vehicles and large-scale electricity storage in smart or intelligent grids [1,2]. Since firstly reported by Padhi et al. [3], olivine-type phosphates $LiFePO_4$ cathode has been made remarkable progress in both research and commercialization. In recent years, $LiMnPO_4$ has become an alternative promising candidate of cathode materials for lithium-ion battery, as it presents a similar capacity (*ca.* 170 mAh g^{-1}) while a higher redox potential (4.1 V *vs.* Li/Li^+) referring to that of $LiFePO_4$ (3.4 V *vs.* Li/Li^+). However, the $LiMnPO_4$ suffers intrinsically from even lower electric and ionic conductivities in comparison with $LiFePO_4$, resulting in a much poorer electrochemical performance [4,5]. Multiple approaches to solve the drawbacks of $LiMnPO_4$, such as reducing the particle size [6,7], carbon-coating [8–10], as well as doping with metal ions [11–14] have been reported.

* Corresponding author. Tel.: +86 592 2085349; fax: +86 592 2183047.
E-mail address: sgsun@xmu.edu.cn (S.-G. Sun).

0378-7753/$ – see front matter © 2013 Elsevier B.V. All rights reserved.
http://dx.doi.org/10.1016/j.jpowsour.2013.01.184

At present, the solid solution $LiMn_xFe_{1-x}PO_4$ that could operate at voltages of 3.5–4.1 V [15] is regarded as a promising material, because this kind material combines the advantages of relative high electrical conductivity of $LiFePO_4$ and relative high voltage of $LiMnPO_4$. Martha et al. [16] and Hong et al. [17] have reported $LiMn_{0.8}Fe_{0.2}PO_4$/C nanoparticles synthesized by solid state reaction with improved capacity and rate performance. Oh et al. [18] synthesized $LiMn_{0.85}Fe_{0.15}PO_4$/C by ultrasonic pyrolysis, which delivered excellent discharge capacity of 150 mAh g^{-1} at 0.5C rate of charge–discharge and 121 mAh g^{-1} at 2C rate. Saravanan [19] obtained $LiMn_{0.5}Fe_{0.5}PO_4$ nanoplates prepared through a simple solvothermal method with a stable long term cycling performance, but the required large number of organic solvent results in exorbitant cost to this method, which is not conducive to large-scale production.

The rheological phase reaction method is often applied to preparation of compounds or materials through solid–liquid rheological mixture, and presents lots of advantages such as the efficient utilization of surface area of the solid particles, the close and uniform contact between solid particle and fluid, the proper heat exchange, and so on [20]. A significant superior character of the rheological phase reaction method consists in less energy consumption than traditional solid-state reaction, and simpler or more economical than those of wet chemical routes, namely hydrothermal synthesis, sol–gel method and precipitation. The rheological phase reaction has been used as an efficient soft green chemistry method to prepare $LiFePO_4$ electrodes or other materials [20–23]. In the current paper, we report for the first time the synthesis of nanoplatelet carbon coated $LiMn_{0.5}Fe_{0.5}PO_4$ solid solution ($LiMn_{0.5}Fe_{0.5}PO_4$/C) by rheological phase reaction. The as-synthesized materials served as cathode of lithium ion battery displayed excellent electrochemical performances. As comparison, $LiMn_{0.2}Fe_{0.8}PO_4$/C and $LiMn_{0.2}Fe_{0.8}PO_4$/C were synthesized through the same process.

2. Experimental

2.1. Synthesis of $LiMn_{0.5}Fe_{0.5}PO_4$/C

The $LiMn_{0.5}Fe_{0.5}PO_4$/C sample was prepared by rheological phase reaction with stoichiometric amounts of lithium carbonate (Li_2CO_3) (AR), manganese carbonate ($MnCO_3$) (AR), ammonium dihydrogen phosphate ($NH_4H_2PO_4$) (AR) and iron (III) phosphate tetrahydrate ($FePO_4 \cdot 4H_2O$) (AR) as starting materials, and a certain amount of stearic acid ($C_{18}H_{36}O_2$) (AR) as carbon source. A solid–liquid rheological body was obtained from starting materials mentioned above under the appropriate quantity of ethanol as dispersant mixed uniformly by planetary ball milling for 10 h. Then a precursor was obtained from the solid–liquid rheological body evaporated solvent in air at 80 °C for 5–8 h. Finally the resulting precursor was thermally treated in a tube furnace at 350 °C for 2 h, then at 600 °C for 5 h under inert atmosphere to yield $LiMn_{0.5}Fe_{0.5}PO_4$/C. $LiMn_{0.2}Fe_{0.5}PO_4$/C, $LiMn_{0.8}Fe_{0.5}PO_4$/C were synthesized according to the aforementioned process with varying the corresponding stoichiometric amounts of Mn and Fe sources.

2.2. Sample characterization

Thermogravimetric analysis was conducted on a simultaneous thermal analysis apparatus (SDTQ600, TA Instruments) to determine the sintering temperature. The precursor of $LiMn_{0.5}Fe_{0.5}PO_4$/C was heated from room temperature to 1000 °C with a heating rate of 10 °C min^{-1}. The measurement was performed in nitrogen flow, using α-Al_2O_3 as reference material. The structure and phases present in the as-synthesized $LiMn_{0.5}Fe_{0.5}PO_4$/C material was identified by powder X-ray diffraction (XRD) patterns recorded on an automated Philips X'Pert Pro Super X-ray diffractometer with Cu kα radiation operating at 40 kV × 40 mA. The 2θ varied from 10 to 70° at a scanning rate of 10° min^{-1}. The lattice constants were determined by Rietveld refinement using the X'pert High Score Plus software. A Nicolet 330 FTIR spectrometer was used to collect the FTIR spectra using KBr pellet techniques. The morphology of $LiMn_{0.5}Fe_{0.5}PO_4$/C particle was observed by scanning electron microscopy (SEM) (HITACHI S-4800), equipped with an energy dispersive X-ray spectroscopy (EDX) that was served to analyze the element content of Mn, Fe, and P. An ICP-MS-4500 instrument was used to determine the element content of Li, Mn, and Fe in $LiMn_{0.5}Fe_{0.5}PO_4$/C. The structure of the $LiMn_{0.5}Fe_{0.5}PO_4$/C samples was also analyzed by a transmission electronic microscopy (TEM) (JEM-2100). The specific surface area of the sample was measured by BET Nitrogen sorption isotherms (Micromeritics Tristar 3000). Vario EL III Elemental analyzer (Elementar Analysen Syeteme GmbH, Germany) was used to control the carbon content of the synthesized materials.

2.3. Electrochemical measurements

Electrodes were prepared by manually mixing the active material, carbon (acetylene black from Alfa), and the binder (LA-133, 14.96 wt %) in a weight ratio of 80:10:10 in deionized water. The slurry was then coated on Al-foil current collectors. The dried electrodes were subsequently assembled into 2025 coin cells in glove box filled with argon using Li metal foil as counter electrode with a microporous polymer separator (Celgard 2400) and liquid electrolyte mixtures (TINCI, Guangzhou), which contains 1 M $LiPF_6$ and a solvent mixture of ethylene carbonate (EC), dimethyl carbonate (DMC) and ethyl methyl carbonate (EMC) (1:1:1, v/v). The electrochemical measurements were performed on the battery test system (Neware BTS, 5 V, 5 mA, Shenzhen) for constant current charge–discharge cycle test. The current density at 1C was based on a capacity of 150 mAh g^{-1}. The test voltage range was between 2.5 V and 4.5 V. All potentials presented in this paper were quoted vs the Li/Li^+ scale.

3. Results and discussion

Fig. 1 shows TG/DTG curves of the precursor at a heating rate of 10 °C min^{-1} from ambient temperature to 1000 °C. It can observe that thermal decomposition of the precursor occurs in two well-defined steps, i.e. at 230 °C and 405 °C, respectively. The observed initial weight loss before 230 °C is attributed to the

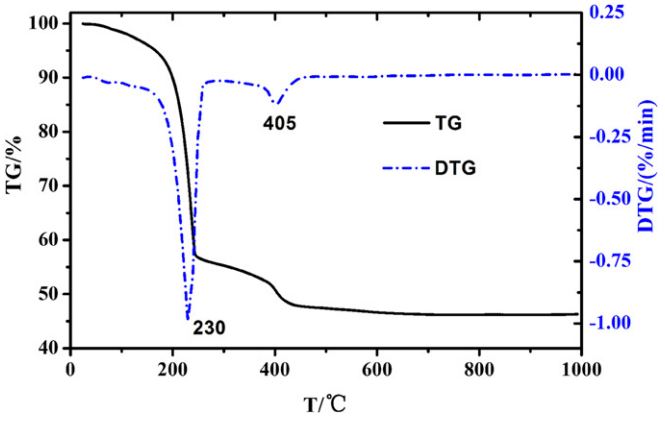

Fig. 1. TG and DTG curves of $LiMn_{0.5}Fe_{0.5}PO_4$/C precursor.

evaporation of stearic acid, initial decomposition of $NH_4H_2PO_4$ and $MnCO_3$, and dehydration of $FePO_4 \cdot 4H_2O$. Another continuous weight loss between 230 °C and 405 °C may be ascribed to the further thermal decomposition precursor compounds as well as the stearic acid. The final weight loss from 405 °C to 600 °C corresponds mainly to the crystallization of product. No weight loss could be observed after 600 °C. In the calcination process, some carbon from degradation of stearic acid lead Fe (III) to be reduced to Fe (II), the residual carbon uniformly coated on the surface of particles. The total weight lose is about 54%, which is near the theoretical value (53.26%). Based on TG/DTG results, we designed the calcination program as follows: a pre-calcination was conducted firstly at 350 °C for 2 h, and then the calcinations were carried out at 600 °C for 5 h. The pre-calcination at 350 °C was aimed to remove sufficiently the crystalliferous water, CO_2 and NH_3 derived from the decomposition of raw materials.

The X-ray diffraction pattern of the as-prepared compound $LiMn_{0.5}Fe_{0.5}PO_4/C$ is displayed in Fig. 2a. All the Bragg diffraction peaks of the compound are well indexed based on a single-phase olivine-type structure in orthorhombic and Pnmb (62) space group (JCPDS No.42-0580). No peaks of impurity phases such as Li_3PO_4, $Mn_2P_2O_7$ mentioned in previous reports [24] could be observed. The residual carbon can't be detected because of the rare content and amorphous configuration. The lattice parameters are estimated to be: $a = 6.049$ Å, $b = 10.393$ Å, and $c = 4.726$ Å, which are close to previously reported values [19].

The FTIR spectrum of $LiMn_{0.5}Fe_{0.5}PO_4/C$ in the 1300–400 cm^{-1} wavenumber range corresponding to the stretching mode of PO_4^{3-} anion is shown in Fig. 2b. The first three bands, i.e. two sharp bands at 1138 and 1095 cm^{-1} and a broad one at 1059 cm^{-1}, are attributed asymmetric stretching mode (υ_3). The band at 997 cm^{-1} is ascribed to symmetric stretching mode (υ_1), and the band near 635 cm^{-1} to asymmetric bending mode (υ_4). The four bands at 579, 551, 501, 469 cm^{-1} correspond to the bending modes (υ_2 and υ_4). It is worthwhile mentioning that the band of υ_1 mode, which indicates the deformation of P–O, has been shifted positively in comparison with that for $LiFePO_4$ (~979 cm^{-1} [25]) and $LiMnPO_4$ (~989 cm^{-1} [26]). This shift reflects the difference in the lattice structure between $LiMn_{0.5}Fe_{0.5}PO_4$ solid solution and $LiFePO_4$ or $LiMnPO_4$. The IR bands below 400 cm^{-1} that are assigned to external modes or lattice vibrations of this compound [25,27] are not presented here.

As illustrated by SEM images in Fig. 3a and b, the $LiMn_{0.5}Fe_{0.5}PO_4/C$ particles display a platelet-like shape with average wide dimension around 115 nm. Simultaneously, some nanoparticles agglomerate into irregular sub-micrometer grains. The as-synthesized materials keep a uniform looser distribution and smaller grain size than that prepared by solid-state reaction consisting of the processes of mechanical mixing and extensive heating at high temperature, which may reduce the specific capacity and cycling performance of electrode materials [28]. This particular structure of $LiMn_{0.5}Fe_{0.5}PO_4/C$ particles is attributed to the crucial role of stearic acid, which acts as a surfactant reducing the surface tension of solid–liquid interface. A Mn/Fe/P ratio of 0.46:0.49:1 is measured by EDX analysis, and a Li/Mn/Fe ratio of 1:0.48:0.47 is confirmed by the ICP-MS measurement. These experimental data are close to the theoretical atomic ratio.

Fig. 3c and d depicts TEM and HRTEM images of $LiMn_{0.5}Fe_{0.5}PO_4/C$ particles, from which we can observe clearly atomic lattice of the $LiMn_{0.5}Fe_{0.5}PO_4$. An amorphous phase of carbon layer with a thickness of around 5 nm covered on the surface of primary particles is observed distinctly in the HRTEM image. This means that the dissolved stearic acid in ethanol solvent could be uniformly mixed with other raw materials to ensure residual carbon distributed homogenously on the surface of $LiMn_{0.5}Fe_{0.5}PO_4$. Elemental analyzer analysis of the $LiMn_{0.5}Fe_{0.5}PO_4/C$ particles indicates that the carbon content of sample is 3.158%. The specific surface area of the pristine $LiMn_{0.5}Fe_{0.5}PO_4/C$ particles measured by N_2 absorption using the Brunauer–Emmett–Teller (BET) model is 22.71 $m^2\ g^{-1}$.

The typical cycling behavior and rate capability of the $LiMn_{0.5}Fe_{0.5}PO_4/C$ electrode at 25 °C in galvanostatic experiments within a voltage range 2.5–4.5 V (*vs.* Li/Li^+) are presented in Figs. 4 and 5. We observe clearly in Fig. 4a and b two voltage platforms in both the charge and discharge curves, one is located at ~3.4 V and another at ~4.1 V, corresponding respectively to the redox plateau potentials of Fe^{2+}/Fe^{3+} and Mn^{2+}/Mn^{3+}. When the charge/discharge rate is increased to 1 C, the platform near 4.1 V becomes shorter than that at 3.4 V, indicating that less capacity is contributed by Mn and confirming a crucial factor in restricting high rate property. To achieve more outstanding capability, much effort on stimulating potential of Mn is absolutely required in future. From the corresponding differential capacity curves (Fig. 4c and d) of first cycle at 0.1C and 1C, two redox peaks representing Mn^{2+}/Mn^{3+} and Fe^{2+}/Fe^{3+} are seen. The peak potential differences between oxidation trace and reduction trace of initial cycle at 0.1C and 1C rate are 0.031 V (Fe^{2+}/Fe^{3+}), 0.063 V (Mn^{2+}/Mn^{3+}), 0.133 V (Fe^{2+}/Fe^{3+}) and 0.281 V (Mn^{2+}/Mn^{3+}), respectively. Obviously, greater polarization appears to 1C rate than 0.1C rate, due to a larger concentration polarization and Ohmic polarization in faster electrochemical reaction at higher charge–discharge current density.

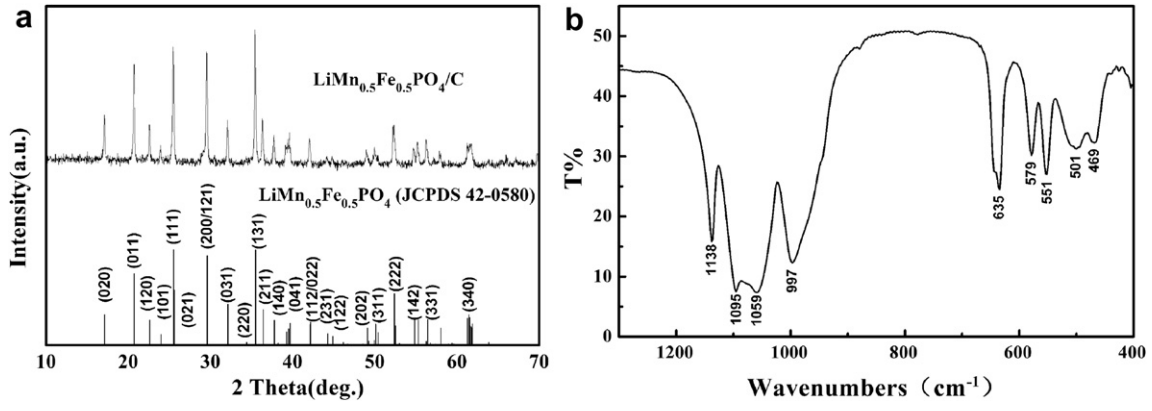

Fig. 2. (a) XRD patterns of solid solutions $LiMn_{0.5}Fe_{0.5}PO_4$ JCPDS standard (card number 42-0580), and $LiMn_{0.5}Fe_{0.5}PO_4/C$ prepared by rheological phase reaction. (b) FTIR spectra of $LiMn_{0.5}Fe_{0.5}PO_4/C$.

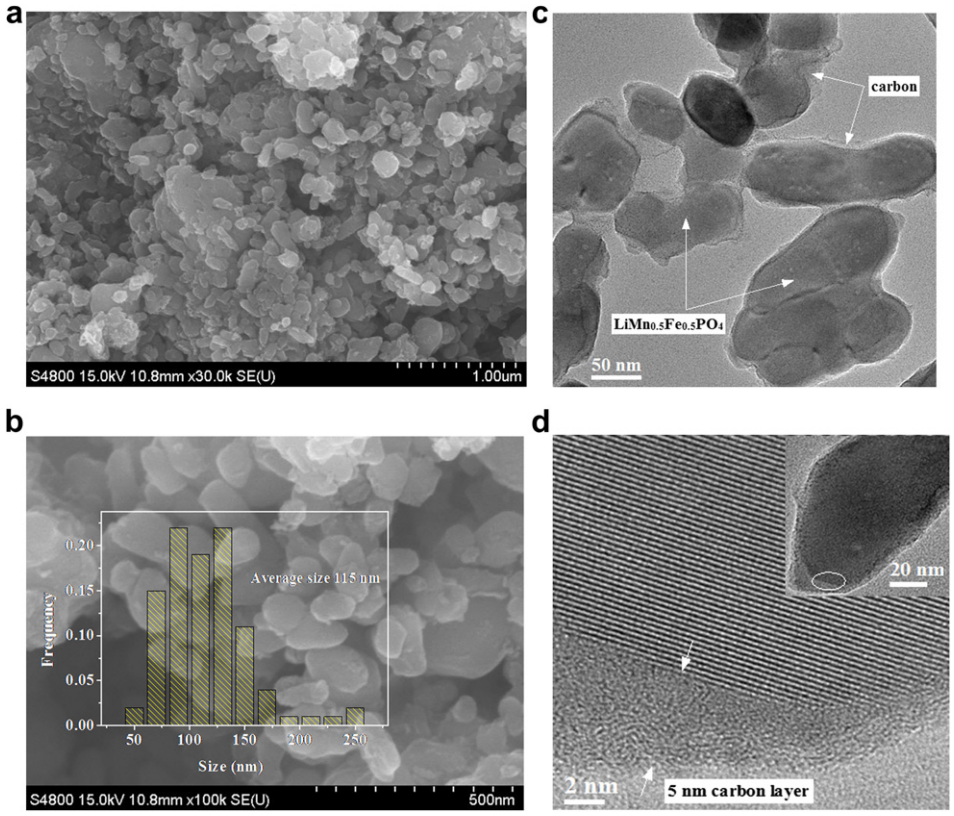

Fig. 3. SEM images (a, b), TEM (c) and HRTEM (d) images of the as-synthesized $LiMn_{0.5}Fe_{0.5}PO_4/C$. The inset in (b) is the statistics of particle size distribution.

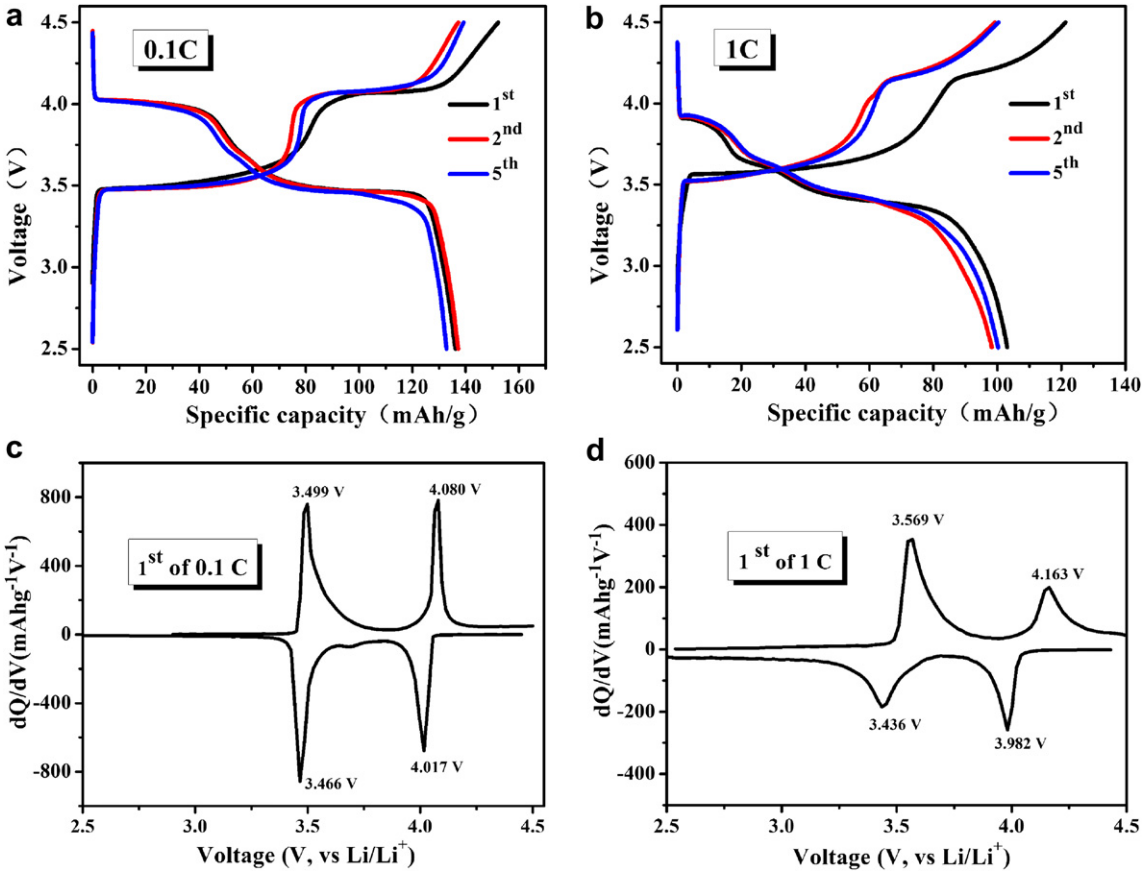

Fig. 4. Charge/discharge curves at 0.1C rate (a) and 1C rate (b) of $LiMn_{0.5}Fe_{0.5}PO_4/C$, differential capacity curves of first cycle at 0.1C rate (c) and 1C rate (d) of $LiMn_{0.5}Fe_{0.5}PO_4/C$.

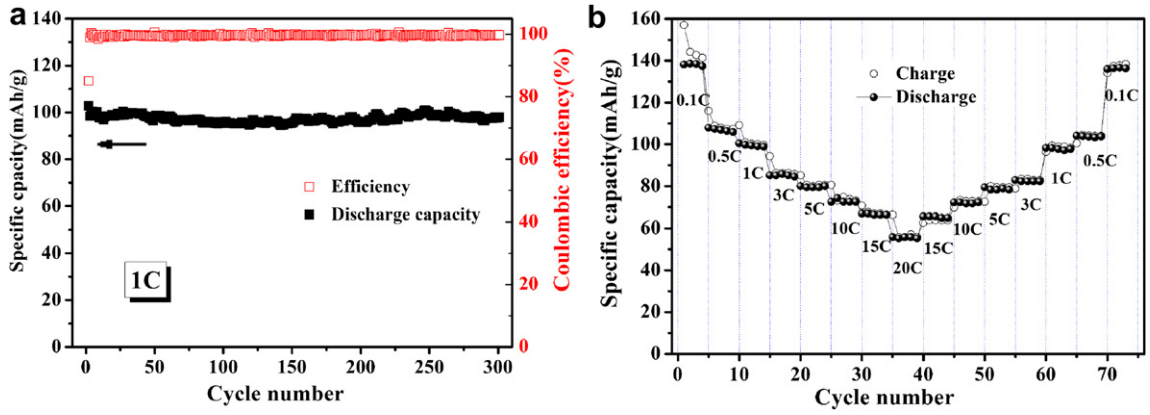

Fig. 5. Electrochemical properties of $LiMn_{0.5}Fe_{0.5}PO_4/C$: (a) cycling capacity of 1C rate, and (b) rate performance during discharged at each C-rates, and then following a constant charge rate at 1C except the same charge/discharge C-rate at 0.1C and 0.5 C.

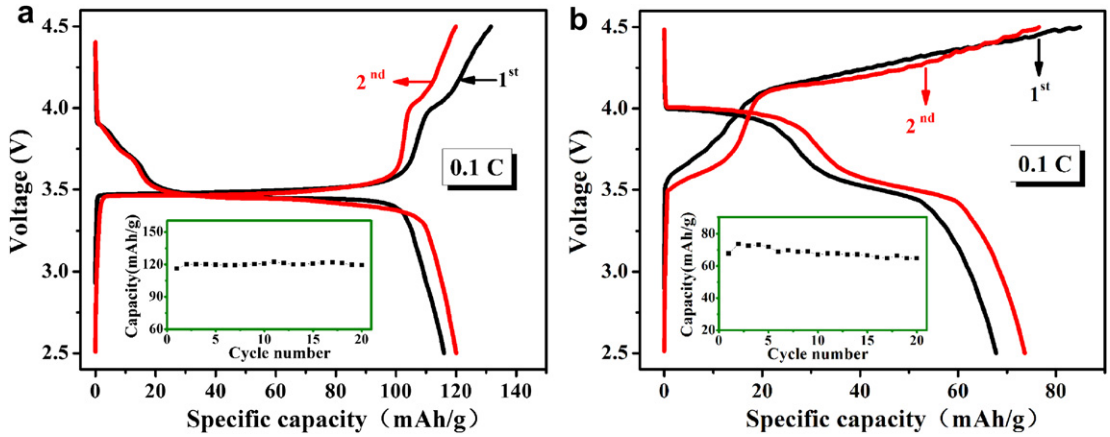

Fig. 6. Charge/discharge curves and capacity cycling performances (insers to figure) at 0.1C of (a), $LiMn_{0.2}Fe_{0.8}PO_4/C$, and (b) $LiMn_{0.8}Fe_{0.2}PO_4/C$.

The cycle performance of the as-prepared $LiMn_{0.5}Fe_{0.5}PO_4/C$ at 1C rate of charged/discharged is showed in Fig. 5a. A good cycling stability is demonstrated with initial specific discharge capacity of 103 mAh g^{-1} and without noticeable capacity fading over 300 cycles. High coulombic efficiency near 100% is reached in 1C rate except the initial cycle (85%), which reveals good reversibility of the material. As illustrated in Fig. 5b, reversible discharge capacities of 138, 99, 80, 72, 67 and 55 mAh g^{-1} have been measured corresponding successively to the 0.1, 1, 5, 10, 15 and 20 C. Capacity can be recovered very well when the current density turns back to low rate after cycling at high rates, indicative of favorable structure stability of the material over cycling even at high current density. It is evident that the overall electrochemical property is closely related with the improvement of electronic conductivity of the material by the evenly coating carbon film on $LiMn_{0.5}Fe_{0.5}PO_4$, which in addition protects the particle surface from HF attack and thus reduces Mn dissolution in the electrolyte [18].

To further investigate the effect of the Mn:Fe ratio in LMFP materials on their electrochemical properties, two samples with Mn:Fe = 0.2:0.8 and Mn:Fe = 0.8:0.2 were synthesized using the same rheological phase reaction. The electrochemical performances of the $LiMn_{0.2}Fe_{0.8}PO_4/C$ and $LiMn_{0.2}Fe_{0.8}PO_4/C$ are illustrated in Fig. 6. Typical voltage profiles of the $LiMn_{0.2}Fe_{0.8}PO_4/C$ at 0.1C and room temperature are shown in Fig. 6a. This cathode has delivered an initial discharge capacity of 116 mAh g^{-1} together with a coulombic efficiency of 89%. From the variation of the discharge capacity vs cycling number (insert to Fig. 6a), we can see that the capacity is maintained at 120 mAh g^{-1} after 20 cycles of charge/discharge. For the $LiMn_{0.8}Fe_{0.2}PO_4/C$ sample at 0.1C (Fig. 6b), two couples of voltage platforms at ~3.4 V and 4.1 V are appeared in charge/discharge curves, respectively. Unsatisfactory initial discharge capacity of only 68 mAh g^{-1} has been determined.

It is obvious that $LiMn_{0.5}Fe_{0.5}PO_4/C$ exhibited the best electrochemical performances among the LMTP materials of different Mn:Fe ratios investigated in the present paper. The superior performances of the $LiMn_{0.5}Fe_{0.5}PO_4/C$ cathode could be ascribed to the small nanoplatelets with uniform distribution, the high specific surface area and the proper balance between the advantages of LMP and LFP.

4. Conclusion

In the current paper, we proposed an economical and uncomplicated rheological phase reaction method to prepare olivine structured solid solution $LiMn_xFe_{1-x}PO_4/C$ (x = 0.2, 0.5, 0.8) composites by stearic acid as carbon source. The as-prepared $LiMn_{0.5}Fe_{0.5}PO_4/C$ presents a well-crystallized nanoplatelet structure and was coated with carbon layer of a few nanometers. The addition of stearic acid into precursor materials plays an important role in mixing uniformly the starting raw materials, and reducing particle size. The later was achieved since the stearic acid acts as both surfactant and carbon source for coating carbon on $LiMn_{0.5}Fe_{0.5}PO_4/C$ particles during thermal treatment. The $LiMn_{0.5}Fe_{0.5}PO_4/C$ composite served as cathode of lithium ion battery exhibits the

best excellent reversible capacities at galvanostatic charge–discharge test amongst the LMFP materials investigated. The specific discharge capacities have been reached 138, 99, 80, 72, 67 and 55 mAh g^{-1} at 0.1, 1, 5, 10, 15 and 20C rate of charge–discharge, respectively. A long stable cycling performance at 1C up to 300 cycles was achieved. The rheological phase reaction synthesis of $LiMn_{0.5}Fe_{0.5}PO_4$/C composite materials combines the advantages of high temperature solid state reaction and wet chemical methods, which processes a short sintering time and consists in a simple, reliable and economic technique.

Acknowledgments

This work was supported by the National Science & Technology Pillar Program of China (No. 2007BAQ01055), and National Nature Science Foundation of China (No. 50574063, No. 21021002 and No. 21003102).

References

[1] A. Stein, Nat. Nanotechnol. 6 (2011) 262.
[2] F.Y. Cheng, J. Liang, Z.L. Tao, J. Chen, Adv. Mater. 23 (2011) 1695.
[3] A.K. Padhi, K.S. Nanjundaswamy, J.B. Goodenough, J. Electrochem. Soc. 144 (1997) 1188.
[4] H.C. Yoo, M.K. Jo, B.S. Jin, H.S. Kim, J. Cho, Adv. Energy Mater. 1 (2011) 347.
[5] A. Yamada, M. Hosoya, S.C. Chung, Y. Kudo, K. Hinokuma, Y.L. Kuang, Y. Nishi, J. Power Sources 119 (2003) 232.
[6] C. Delacourt, P. Poizot, M. Morcrette, J.-M. Tarascon, C. Masquelier, Chem. Mater. 16 (2004) 93.
[7] S.K. Martha, B. Markovsky, J. Grinblat, Y. Gofer, O. Haik, E. Zinigrad, D. Aurbach, T. Drezen, D. Wang, G. Deghenghi, I. Exnar, J. Electrochem. Soc. 156 (2009) A541.
[8] Z. Bakenov, I. Taniguchi, J. Power Sources 195 (2010) 7445.
[9] S.-M. Oh, S.-W. Oh, C.-S. Yoon, B. Scrosati, K. Amine, Y.K Sun, 20 (2010) 3260.
[10] Z. Bakenov, I. Taniguchi, Electrochem. Commun. 12 (2010) 75.
[11] T. Muraliganth, A. Manthiram, J. Phys. Chem. C 114 (2010) 15530.
[12] G. Yang, H. Ni, H.D. Liu, P. Gao, H.M. Ji, S. Roy, J. Pinto, X.F. Jiang, J. Power Sources 196 (2011) 4747.
[13] J. Kim, Y.-U. Park, D.-H. Seo, J. Kim, S.-W. Kim, K. Kang, J. Electrochem. Soc. 1583 (2011) A250.
[14] G.Y. Chen, A.K. Shukla, X.Y. Song, T.J. Richardson, J. Mater. Chem. 26 (2011) 10126.
[15] A. Yamada, S.C. Chung, J. Electrochem. Soc. 148 (2001) A960.
[16] S.K. Martha, J. Grinblat, O. Haik, E. Zinigrad, T. Drezen, J.H. Miners, I. Exnar, A. Kay, B. Markovsky, D. Aurbach, Angew. Chem. Int. Ed. 48 (2009) 8559.
[17] J. Hong, F. Wang, X.L. Wang, J. Graetz, J. Power Sources 96 (2011) 3659.
[18] S.-M. Oh, H.-G. Jung, C.S. Yoon, S.-T. Myung, Z.H. Chen, K. Amine, Y.-K. Sun, J. Power Sources 196 (2011) 6924.
[19] K. Saravanan, V. Ramar, P. Balaya, J.J. Vittal, J. Mater. Chem. 21 (2011) 14925.
[20] C.J. Cong, L. Liao, J.C. Li, L.X. Fan, K.L. Zhang, Nanotechnology 16 (2005) 981.
[21] H. Tang, C.Q. Feng, Q. Fan, T.M. Lei, J.T. Sun, L.J. Yuan, K.L. Zhang, Chem. Lett. 8 (2002) 822.
[22] L.N. Wang, X.C. Zhan, Z.G. Zhang, K.L. Zhang, J. Alloys Compounds 456 (2008) 461.
[23] Y.H. Huang, H.B. Ren, Y.Y. Sheng, Y.H. Wang, Z.H. Peng, Y.H. Zhou, J. Power Sources 195 (2010) 610.
[24] V. Koleva, R. Stoyanova, E. Zhecheva, Mater. Chem. Phys. 121 (2010) 370.
[25] M. Maccario, L. Croguennec, B. Desbat, M. Couzi, F.L. Cras, L. Servantd, J. Electrochem. Soc. 155 (2008) A879.
[26] Y. Bai, F. Wu, C. Wu, Chin. J. Light Scatter. 15 (2003) 231.
[27] C.M. Burba, R. Frech, J. Electrochem. Soc. 151 (2004) A1032.
[28] H. Tang, M.Y. Xi, X.M. Huang, C.Q. Feng, Y. Zhang, K.L. Zhang, J. Mater. Sci. Lett. 21 (2002) 999.